Photoinitiated Reaction Dynamics between Aligned Adsorbates on Solid Surfaces: A Theoretical Exploration of the H + CO_2 System on LiF(001)

Josie V. Setzler and Hua Guo*

Department of Chemistry, University of Toledo, Toledo, Ohio 43606-3390

George C. Schatz

Department of Chemistry, Northwestern University, Evanston, Illinois 60208-3113

Received: January 10, 1997; In Final Form: May 5, 1997[⊗]

We report a quasi-classical trajectory study of a chemical reaction between H and CO_2 at the LiF(001) surface. The reaction is initiated by photodissociation of well-aligned HBr(ad) at 193 nm, which produces a "hot" H atom directed toward a nearby CO_2(ad). Single molecules of each reactant are placed on a static surface, and a full-dimensional HCO_2 potential derived from *ab initio* calculations is used. The adsorbate−substrate and the adsorbate−adsorbate potentials consist of both nonelectrostatic and electrostatic contributions. Several energetically favorable adsorption configurations are determined by a Monte Carlo method. Quasi-classical trajectories are calculated at 80 K for four different adsorption configurations. We find that the reactivity at some configurations is significantly enhanced compared with the corresponding gas-phase simulation. The calculated impact parameters and incident angles of the surface-aligned collisions indicate that the enhanced reactivity can be largely attributed to the closeness and alignment of the coadsorbates on the surface. Owing to the long-lived complex, product distributions, with the exception of a departure angle, show little memory with regard to the initial configuration and are similar to those obtained in the gas phase. A significant number of the unreacted hydrogen atoms retain sufficient energy to make subsequent reaction with other coadsorbates a possibility. We find evidence of several dynamic features pertinent to the use of the surface as a template for reactivity enhancement, including scattering at the surface, the squeezed atom effect, chattering, and caging.

I. Introduction

Although the importance of solid catalysts has been realized for a long time, the advent of high vacuum and laser techniques has only recently made possible unequivocal characterization of many surface processes.[1] Research in the area of surface chemistry has concentrated on adsorption, desorption, scattering, and chemical reactions on various surfaces. Microscopic knowledge of adsorbate−substrate interactions and pertaining dynamics not only sheds light on the surface chemical and physical events on the molecular scale but also allows us to manipulate and design new materials and new chemical reaction routes. Developments in this field will certainly have a significant impact on science and technology in the next century. In this work, we are concerned with the possibility of enhancing the reactivity of a chemical reaction using inert surfaces as templates.

Chemical reaction dynamics involving small gas-phase molecules has been a subject of extensive investigation in the past few decades.[2] It is well established that most reactions will occur when two major criteria are satisfied: the two reactants have to be close enough upon impact to ensure reaction and their relative alignment has to be favorable for the reactive complex to approach a minimum energy pathway. Furthermore, the relative collisional energy has to be higher than the reaction barrier. In fact, dynamical stereochemistry has attracted much attention in the past decades.[2,3] In bulk gaseous conditions, the motion of the reactants is completely random. Consequently, many encounters between the reactants result in nonreactive collisions. In this respect, the gas-phase reaction approach has low efficiency. Little can be done to control the reaction rate other than varying the temperature and/or pressure of the reaction vessel.

The application of lasers alleviates some of the problems for gas-phase reactions. For example, a laser can be used to selectively excite a vibrational mode of a reactant, which may lead to an increase in reaction yield and to different products. Control over final products has been demonstrated in some systems.[4,5] However, this approach is inherently limited to a group of molecules that possess the so-called "local modes". For the majority of molecules, intramolecular vibrational energy redistribution (IVR) is usually too fast to maintain energy localization before reaction can take place. One can also use polarized lasers or other techniques to initiate reactions in bulk by preferentially aligning the reactants before collision. For example, a reaction may take place when one reactant is generated in situ by photodissociation of a molecule in a gas mixture.[6] Sometimes molecules can also be oriented by an external electromagnetic field.[7]

While some control over the alignment of the reactants can be imposed, in gas-phase collisions there is no easy way to select the impact parameter in a collisional process. Recently, Wittig and co-workers[8−10] demonstrated an interesting scheme to control both the alignment and the impact parameter in a chemical reaction. They first generated a precursor cluster in which two reactants are held in close proximity by weak van der Waals forces. Then, the photodissociation of one constituent molecule ejects a fragment toward the other molecule in the complex. An example of such systems is HX·CO_2, where X = Cl, Br, and I. The photodissociation of HX produces a hydrogen atom with a kinetic energy of 1−3 eV, which reacts with CO_2 to produce HO and CO. It was observed that the

* Corresponding author.
[⊗] Abstract published in *Advance ACS Abstracts,* June 15, 1997.

S1089-5647(97)00178-8 CCC: $14.00

OH rotational state distributions from this approach are measurably different from those obtained in the bulk, while its vibrational distribution is invariant. Wittig's scheme has some attractive features. For example, the weak intermolecular forces cause only a small perturbation to the electronic structure of the constituent molecules in the complex. The alignment of the reactants in the van der Waals complex allows detailed examination of the entrance channel specificity and stereochemical selectivity of the reaction. Furthermore, the reaction can be initiated at a prespecified time and energy. Extensive theoretical studies for the HX·CO_2 system have been performed.[11,12]

Similar objectives can be achieved in physisorbed systems on inert solid surfaces. The so-called surface-aligned photoinitiated reaction scheme was first suggested by Polanyi.[13] Analogous to the van der Waals paradigm, the introduction of an insulator surface allows the adsorbed reactants to be held in close proximity to each other. In addition to the intermolecular forces, the adsorbate−substrate interactions provide additional restraints to the precursor complex. Because of the weak adsorbate−substrate interactions, the presence of the surface does not significantly alter the chemical properties of the adsorbed molecules. The bandgap of the substrate is sufficiently large that photoabsorption will be confined to the adsorbate. Thus, the surface serves as an ideal template for the reaction. The adsorption of small molecules on insulator surfaces has been extensively investigated, and many of their adsorption configurations are known. The photodissociation dynamics of adsorbates has also been thoroughly investigated.[14,15] In fact, a number of photoinitiated chemical reactions between coadsorbates have been observed on several insulator surfaces,[16−18] and theoretical explorations have been carried out as well.[18,19] Particularly relevant to the present work is a classical trajectory study of reactions between photolytically prepared H and coadsorbed HBr at LiF(001).[19]

In this work, we report a classical trajectory study on a surface-aligned photoreaction between two coadsorbed molecules on an insulator surface. Specifically, we are interested in the reaction between a "hot" H atom prepared by photodissociation of an adsorbed HBr and a nearby CO_2. The rationale for our selection is explained as follows. First, this system resembles the much studied van der Waals complex HBr·CO_2.[8−10] The so-called HOCO (H + CO_2) system has been under close scrutiny on the experimental front because of its importance in combustion and atmospheric chemistry.[8−10,20−24] An accurate many-body expansion potential for the HOCO system has been developed based on *ab initio* calculations.[25−27] Theoretical studies of the dynamics have been reported for both the forward and reverse reactions.[11,12,25−30] The understanding of the complex multidimensional process in the gas phase and in van der Waals complexes provides a good comparison for the corresponding process on surfaces.

Second, the adsorption of HBr and CO_2 on insulator surfaces has been studied both experimentally and theoretically. For example, it is known that HBr adsorbs on the LiF(001) surface with a tilt angle of ∼21° relative to the surface plane.[31] The H moiety is believed to bind a surface fluorine anion via a hydrogen bond, as evidenced by a red-shift in the adsorbate vibrational frequency.[31] Since the adsorption is site-specific, the mobility of HBr on the surface is limited. Monte Carlo simulations have been performed for this system based on empirically determined interactions and the results gave an excellent agreement with experiments.[32,33] The adsorption energy is about 0.27 eV[34] and is dominated by the electrostatic interaction between the hydrogen and a surface anion.[32,33]

The adsorption of CO_2 on a similar surface (NaCl) has been extensively investigated.[35−40] The molecule was found to adsorb in an orientation near parallel to a Na−Cl axis with a 22° tilt angle relative to the surface plane at monolayer coverage.[35] The adsorption energy of a monolayer of CO_2 on NaCl(001) is approximately 0.25 eV.[36] At low coverage the CO_2 molecule is thought to adsorb parallel to the surface midway between adjacent cations with the oxygen atoms directed toward the cations. Theoretical models have been developed for the system.[38,41,42] To our best knowledge, neither experimental nor theoretical data, other than the calculation of dispersion and repulsion coefficients,[43] are known for the structure of CO_2 on LiF. We expect the adsorption geometry to be similar to that on NaCl.

Our theoretical model represents the first step toward a better understanding of the HBr/CO_2/LiF system. A number of approximations are imposed in this work. First, a static surface is assumed, which precludes energy exchange between the adsorbate and substrate. It is a reasonable approximation, as evidenced by an earlier trajectory study of HBr photodissociation on LiF(001) in which inefficient energy transfer between the H fragment and the substrate was observed.[33] Second, we include only two molecules on the surface. The interaction with nearby adsorbate is modeled with an artificial anchoring potential which allows vibration on the surface consistent with monolayer CO_2 coverage. Some of these admittedly simplified assumptions will be removed in future work. This paper is organized as follows: the theoretical model and the interaction potential are presented in the next section (section II). The simulation methods, including both the Monte Carlo and quasi-classical trajectory methods, are briefly discussed in section III. The calculated results are presented in section IV. Particular attention is paid to the elucidation of reaction dynamics and final state distributions from the perspective of the initial adsorbate alignment. Finally, discussion and concluding remarks are presented in section V.

II. Theoretical Model and Interaction Potential

In this work, we employ a static surface approximation in which all the surface ions are fixed at their equilibrium positions. A single molecule of each reactant, HBr and CO_2, is included in the simulation. The total potential energy of the system can be separated into adsorbate−substrate, adsorbate−adsorbate and intraadsorbate interactions:

$$V = V_{as} + V_{aa} + V_m \tag{1}$$

The adsorbate−substrate interaction consists of the classical electrostatic interaction and the core interactions due to dispersion and short-range Pauli repulsion. The core interaction is calculated as the sum of all the pairwise atom−atom interactions. For HBr, we use the simple Lennard-Jones 6−12 potential to represent the interatomic interactions:

$$V(r) = 4\epsilon\left[\left(\frac{\sigma}{r}\right)^{12} - \left(\frac{\sigma}{r}\right)^{6}\right] \tag{2}$$

where r is the internuclear distance. The parameters ϵ and σ are adopted from an earlier work from our group[33] and are listed in Table 1. To correctly reproduce the hydrogen bond between the adsorbate and surface, the value of σ_{H-F} is adjusted to 2.4 Å, producing a tilt angle and binding energy consistent with experiment.[33] The scattering of H from the surface is considered to be nonreactive, which is justified by experimental findings for the dissociation of HBr on LiF(001).[34]

The core interaction between CO_2 and the surface is represented by the sum of the pairwise atom−atom potentials

TABLE 1: Parameters for Interaction Potentials

(I) Adsorbate-Surface Interaction

(a) HBr−Surface Interaction Parameters (Eq 2)

interaction	ϵ (meV)	σ (Å)
H−Li^+	0.027	3.44
H−F^-	1.09	2.44
Br−Li^+	0.62	3.10
Br−F^-	15.7	2.96

(b) CO_2−Surface Interaction Parameters (Eq 3)

interaction	C_6 (eV Å^6)	C_8 (eV Å^8)	C_{10} (eV Å^{10})	B (eV Å^{12})
C−Li^+	0.9424	1.028	1.395	7.988×10^3
O−Li^+	0.8506	0.8993	1.184	4.450×10^3
C−F^-	34.317	37.433	50.815	3.863×10^4
O−F^-	30.969	32.755	43.111	2.072×10^4

(II) Adsorbate−Adsorbate Interaction Parameters (Eq 6)

interaction	C_6 (eV Å^6)	b (eV)	β (Å^{-1})
C−H	5.616	264.3	3.144
C−Br	54.27	4135.	3.198
O−H	3.359	444.7	3.544
O−Br	32.46	6958.	3.598

(III) Partial Charges and Polarizability (Eq 4)

	C	O	H	Br	ghost atom
q_i (e$^-$)	0.54	−0.27	0.276	−0.444	0.168
α_i (Å^3)	0.96	0.84	0.67	3.05	

(IV) Intramolecular Potential of HBr (Eq 8)

	a (eV)	γ (Å^{-1})	ϵ (eV)
$^1\Pi_1$	61.2	2.01	0.0
$^3\Pi_{0^+}$	223	3.01	0.457

(V) Anchoring Potential for CO_2 (Eq 9)

	position			
x_0 (Å)	0.0	1.0	1.0	2.1
y_0 (Å)	−1.66	−1.17	−2.97	−0.22
ϕ_0 (deg)	90	135	45	0
$k_x = 0.0247$ eV Å^{-2}				
$k_y = 0.0247$ eV Å^{-2}				
$k_\phi = 0.0270$ eV				

given by the following expression:

$$V(r) = -\frac{C_6}{r^6} - \frac{C_8}{r^8} - \frac{C_{10}}{r^{10}} + \frac{B}{r^{12}} \tag{3}$$

where C_6, C_8, and C_{10} are the Kirkwood−Müller dispersion coefficients and B is the repulsive coefficient. Values for these coefficients are adopted from the work by Heidberg et al.[43] and are also listed in Table 1.

The electrostatic part of the adsorbate−substrate interaction includes both Coulombic interaction between the charged particles and the induction energy:

$$V = \sum_{i=1}^{6} q_i \Phi_s(\mathbf{r}_i) - \frac{1}{2}\sum_{i=1}^{5} \alpha_i [\nabla \Phi_s(\mathbf{r}_i)]^2 \tag{4}$$

where the electrostatic potential above the ideal semiinfinite ionic crystal is obtained from an expression suggested by Steele:[44]

$$\Phi_s(\mathbf{r}) = \frac{16q}{\sqrt{2}a} \frac{e^{-2\sqrt{2}\pi z/a}}{1 + e^{-\sqrt{2}\pi}} \cos\left(2\pi\frac{x}{a}\right)\cos\left(2\pi\frac{y}{a}\right) \tag{5}$$

where a is the lattice constant set at 3.98 Å for LiF(001).[33] The two-dimensional unit cell has cations of charge $+q$ positioned at (0, 0) and (a/2, a/2) and anions of charge $-q$ at (a/2, 0) and (0, a/2). The atomic partial charges in CO_2 are taken from Heidberg et al.[41] HBr is also represented by three point charges residing on the two nuclei and a ghost atom 1.292 Å from Br on the molecular axis on the opposite side of H, as suggested by Polanyi et al.[32] The second term in eq 4 is usually much smaller than the first term. The partial charges (q_i) and polarizabilities (α_i) are given in Table 1.

The adsorbate−adsorbate potential is also expressed as a sum of electrostatic and nonelectrostatic contributions. The core potential between the HBr and CO_2 molecules is represented as the pairwise sum of a dispersion term and an exponential repulsive term:

$$V(r) = \frac{-C_6}{r^6} + be^{-\beta r} \tag{6}$$

The parameters, shown in Table 1, were calculated from atom−atom potentials determined by Spackman[45] using the Gordon−Kim electron gas model. The electrostatic interaction is handled by using a point-charge model for the electronic charge distribution of the adsorbate molecules:

$$V = \sum_{i=1}^{3}\sum_{j=1}^{3} \frac{q_i q_j}{r_{ij}} \tag{7}$$

In the Monte Carlo simulation before the absorption of the photon, the HBr and CO_2 are modeled as two separate, rigid molecules on the surface and the ground-state adsorbate−adsorbate potential is represented by the pairwise interactions described above. Upon photoabsorption, the excited-state potential of the system is given by a sum of the excited-state HBr potential and the potential for the HOCO complex. The potentials of HBr are taken from the gas-phase data. The ground electronic state is represented by a Morse potential, while the two repulsive excited states are represented by exponential functions[33] fitted to an earlier *ab initio* calculation:[46]

$$V(r) = ae^{-\gamma r} + \epsilon \tag{8}$$

The corresponding parameters are given in Table 1.

For the excited state, the interaction between Br and CO_2 is represented by a pairwise sum of Lennard-Jones atom−atom potentials. This is a reasonable assumption and has been used in previous simulations.[12] The HOCO potential used in our calculations is a modified version of the global analytical potential developed by Schatz and co-workers for the HOCO system.[25,26] The schematic reaction pathways of this well-studied reaction are shown in Figure 1. The near-collinear H attack leads to *cis*- and *trans*-HOCO complexes, while the perpendicular entrance channel results in a T-shaped complex which can isomerize to the HOCO complex over a high barrier. Figure 2 shows a contour plot drawn as a function of H-atom Cartesian coordinates relative to the center of mass of CO_2. At each H atom location the CO_2 bend and stretch coordinates are adjusted to minimize the energy. The O−O axis is placed parallel to the abscissa, and all four atoms are coplanar. The U-shaped contours around each O atom correspond to the HOCO cis and trans minima, while the circular contours near the C atom indicate the HCO_2 minimum. The details of the potential can be found in the original publication,[25,26] and no further information is given here. The core interaction for the HOCO complex with the substrate is treated as a pairwise sum of atom−atom potentials, just as it is for the adsorbate molecules before excitation. The electrostatic interaction between the

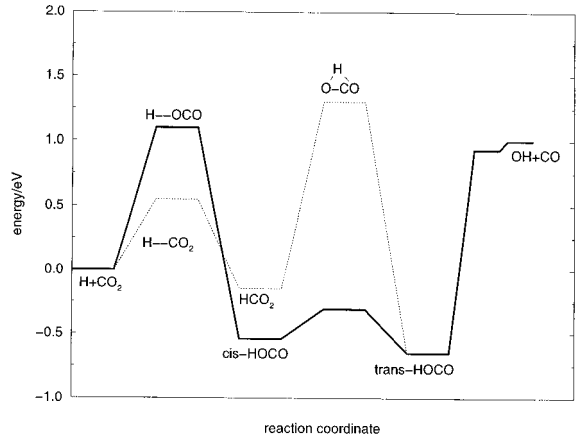

Figure 1. Schematic reaction pathways for the H + CO_2 ↔ OH + CO system. The solid and dashed lines indicate the near collinear and T-shaped pathways, respectively.

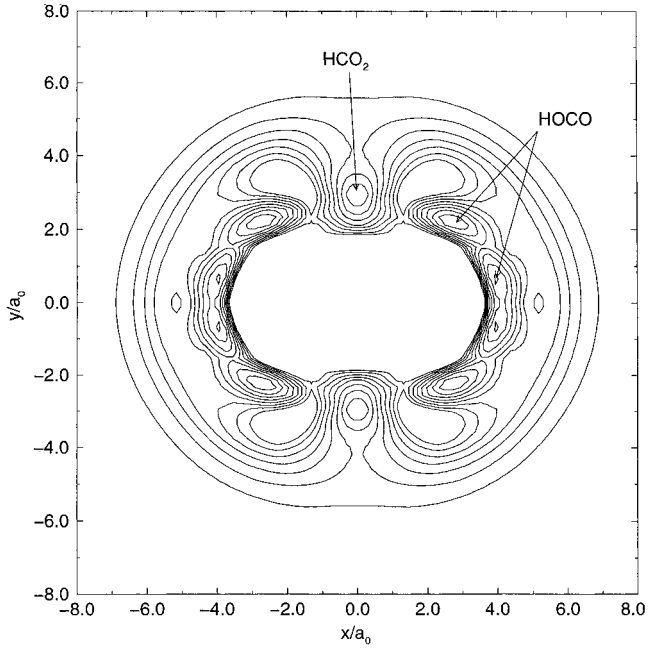

Figure 2. Contour plot of the HOCO potential energy surface as a function of the Cartesian coordinates (x,y) of the H atom, with CO_2 along the x axis. The total energy of the system is minimized for each point.

complex and the surface is neglected due to the lack of information on the charge distribution of the complex.

III. Simulation Methods

The simulation is carried out in two steps, similar to previous quasi-classical trajectory studies of photodissociation of adsorbates on insulator surfaces.[33,47−49] First, the adsorbates are equilibrated at a given temperature (typically 80 K) using the Metropolis Monte Carlo (MC) method.[50] In the MC simulation, the molecules are treated as rigid skeletons, and both the center of mass and the orientation of the molecules with respect to the surface are varied randomly in search of an energy minimum. Typically, the system relaxes into an equilibrium configuration in less than 5000 steps. After equilibration, the adsorption energy and average positions are calculated. The positions of the adsorbates at every 50 steps afterward are saved as initial conditions for the subsequent trajectory calculations.

The photoinduced reaction dynamics is simulated by quasi-classical trajectories. The CO_2 molecule is prepared in its ground vibrational state and the initial atomic Cartesian coordinates and velocities are assigned by transforming the normal coordinates and momenta with randomly selected initial phase angles at the ground vibrational state.[51] The initial rotational angular momentum of CO_2 is set to zero, as are the center of mass velocities. Photodissociation of the HBr molecule at 193 nm is simulated by promoting the molecule from the ground state to the $^1\Pi_1$ repulsive excited state via a Franck−Condon transition. The initial interatomic distance at which HBr absorbs the photon is determined from the Wigner probability distribution for the ground-state HBr. The functional form and parameters of the Wigner distribution are adopted from an earlier calculation.[33] The excess energy ($h\nu - V(q)$) is converted to kinetic energy in the dissociation coordinate. In the gas phase, the dissociated H fragment in the $^1\Pi_1$ ($^3\Pi_{0+}$) channel should have a kinetic energy of 2.61 (2.11) eV.

Hamilton's equations are solved numerically using a velocity Verlet algorithm.[50] The derivatives of the HOCO potential are calculated using a finite differencing method, while the derivatives of all the other potentials are obtained analytically. The size of the time step is checked to ensure convergence of the propagation and conservation of energy. For the results reported here, a time increment of 4 au (∼0.1 fs) is found to yield satisfactory results. Nonadiabatic transitions between the two electronic states in HBr are simulated by using the surface hopping scheme of Tully and Preston.[52] When the propagation reaches the crossing point of the two diabatic excited-state surfaces, the nonadiabatic transition probability is calculated using the semiclassical Landau−Zener formula.[53] The coordinate-independent coupling strength was chosen[33] to yield a transition probability of 15%, which is the experimental ratio for the two spin−orbit channels.[34] The propagation is terminated when three or more of the six interatomic distances among the adsorbate atoms are greater than 12 bohr apart. The products of the trajectory are then assigned as either CO + OH or H + CO_2, based on a comparison of the interatomic distances. No zero-point energy correction is imposed. We focus on the reactive channel although some results in the nonreactive channel will also be presented. The final rotational and vibrational quantum numbers of the reactive products (CO + OH) are determined using the conventional binning procedure.[54] Approximately 1000 trajectories are calculated for each adsorption configuration. The total time of propagation ranges from less than 100 fs for direct scattering to as much as 1 ps for complex forming trajectories. Because the unequivocal determination of desorption of an adsorbate is extremely time consuming, we use a simple criterion. A product is considered desorbed if its z-component velocity is positive at the end of propagation. Although this criterion for desorption is obviously a crude approximation, it does give an upper limit for the desorption probability.

IV. Results

(A) Adsorption Configurations. The Monte Carlo study found that the HBr aligns along the Li^+−F^- axis with the Br atom above the Li^+ ion and H pointing toward the F^- ion. The tilt angle relative to the surface plane is 25 ± 2°, in reasonably good agreement with experiment[31] as well as earlier MC simulations.[32,33] The HBr adsorption energy of 0.27 eV is also consistent with earlier work. At 80 K, the HBr molecule finds its equilibrium position quickly and does not move across the surface. By contrast, the CO_2 molecule diffuses among many shallow local minima scattered widely around the HBr molecule. No reliable global minimum could be found. The relatively high mobility of CO_2 is probably due to the lack of coadsorbed CO_2. To locate the deepest adsorption configurations, a MC calculation was performed at 0 K. The motion of the HBr molecule is minimal near its adsorption site, while the CO_2

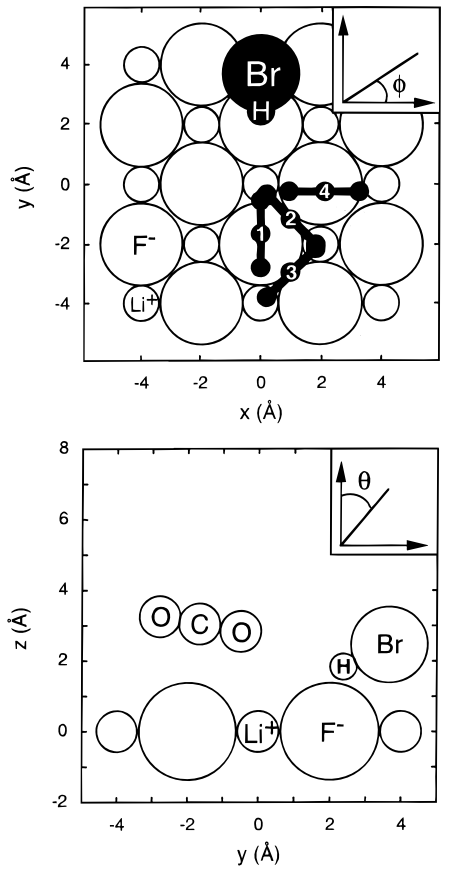

Figure 3. Minimum energy positions for the HBr/CO_2 system on LiF-(001) determined by a MC simulation at 0 K. The position of HBr is anchored by a strong hydrogen bond with the substrate anion while the CO_2 is relatively mobile. The upper panel displays the top view of the absorption configuration of four lowest energy minimum positions, while the side view of position 1 is given in the lower panel. The angles are defined in the inserts. In both panels, ionic crystal radii are used for the substrate ions while the adsorbate atom radii are chosen arbitrarily.

TABLE 2: Minimum Energy Adsorption Configurations at 0 K

	center of mass position			orientation (deg)	
	x (Å)	y (Å)	z (Å)	ϕ	θ
HBr	0.00	3.03	2.15	90	114.9
CO_2 position					
1	0.00	−1.66	3.04	90	100
2	1.00	−1.17	2.91	135	92
3	1.00	−2.97	2.91	45	91
4	2.10	−0.22	3.04	0	94

molecule is allowed to relax into a favorable configuration in an area around the HBr molecule which is likely to be sampled by the photolytically prepared hydrogen atom. Seven lowest energy configurations were identified, four of which are shown in Figure 3. The HBr molecule lies along the *y*-axis, and the CO_2 positions are arranged symmetrically about this axis. The four configurations located in the right half of the figure were chosen for the simulation of the photoreaction and are labeled numerically in the figure. The equilibrium geometry for each of these positions at 0 K is given in Table 2.

The adsorption energy of the four positions displayed in Figure 3 is similar, as shown in Table 3. The major contribution comes from the adsorbate−substrate electrostatic interaction. The short-range core interaction is also substantial for the adsorbate−substrate interaction. The adsorbate−adsorbate interaction is, on the other hand, relatively small. The deepest well (−0.493 eV), located at position 2, situates the CO_2 molecule straddling the space between two cations, maximizing

TABLE 3: Adsorption Energy (eV) of HBr/CO_2 on LiF at 0 K

position	E_{ad}	E_{as}^{core}	E_{as}^{elec}	E_{as}^{ind}	E_{aa}^{core}	E_{aa}^{elec}
1	−0.485	−0.168	−0.243	−0.055	−0.003	−0.016
2	−0.493	−0.184	−0.240	−0.056	−0.001	−0.012
3	−0.483	−0.183	−0.243	−0.056	−0.002	+0.001
4	−0.480	−0.171	−0.239	−0.056	−0.007	−0.007

the electrostatic interaction between the cations and the partial negative charge on the oxygen atoms. The molecule is nearly parallel to the surface, similar to the configuration found by calculations for CO_2 adsorbed on NaCl at low coverage.[41] This configuration also allows for favorable interaction with the coadsorbed HBr. Position 3 is aligned similarly with respect to the surface, but it experiences less interaction with HBr. By contrast, in positions 1 and 4, CO_2 is not aligned with the cations, apparently due to interaction with HBr. In both positions, the carbon atom is near an anion. Position 1 aligns both CO_2 and HBr along the *y*-axis. CO_2 is tilted about 10° with respect to the surface and is pointed down toward the hydrogen atom, producing a favorable H−O configuration. For position 4, the CO_2 molecular axis is perpendicular to the axis of HBr. The latter two positions resemble the structure found for monolayer coverage of CO_2 on NaCl.[35]

At the temperature of our simulation (80 K), an artificial anchoring potential is introduced in the MC simulation to constrain the CO_2 molecule near the minimum energy positions obtained at 0 K. The anchoring potential can be viewed as a substitute for the actual adsorbate−adsorbate interaction between coadsorbed CO_2 molecules at monolayer coverage. It is designed to allow vibrational motion around the equilibrium position consistent with experimental observations. For simplicity, we use the harmonic form:

$$V_a = {}^1/_2 k_x (x - x_0)^2 + {}^1/_2 k_y (y - y_0)^2 + {}^1/_2 k_\phi (\phi - \phi_0)^2 \quad (9)$$

where x and y are the center of mass coordinates of CO_2 and ϕ is the angle in the plane of the surface. The force constants are selected based on spectroscopic observations of the CO_2/NaCl system.[38] The equilibrium positions and force constants are given in Table 1. The *z*-coordinate of the center of mass and the angle with respect to the surface normal were allowed to relax without any constraints. This approximation can be relaxed by introducing a monolayer of CO_2 on the surface.

(B) Reaction Dynamics. *(a) Enhancement of Reactivity.* A quasi-classical trajectory simulation of the reaction was performed for each of the four adsorption configurations on the surface. Two of the four configurations tested yield an enhancement of the reactivity relative to that produced by the corresponding gas-phase simulation (∼2%).[12] In position 1 the number of reactive trajectories was found to be 13.8% of the total number of trajectories, a 7-fold enhancement of the gas-phase results. Position 2 also produces a large number (8.4%) of reactive trajectories. Positions 3 and 4 yield virtually no reactive trajectories, because of unfavorable alignments and positions. Our results indicate that reaction occurs for both slow and fast H atoms produced via nonadiabatic curve-crossing during the dissociation of HBr.

To understand the origin of the enhanced reactivity, we focus on two fundamental quantities for the collisional process: the impact parameter (b) and the incident angle (α). The impact parameter is defined as the perpendicular distance between the incoming hydrogen trajectory and a parallel line passing through the center of mass of the CO_2 molecule. The incident angle is the angle formed between the O−O vector of CO_2 and the velocity vector of hydrogen. These parameters for the surface reaction are not as clearly defined as in the gas-phase reaction

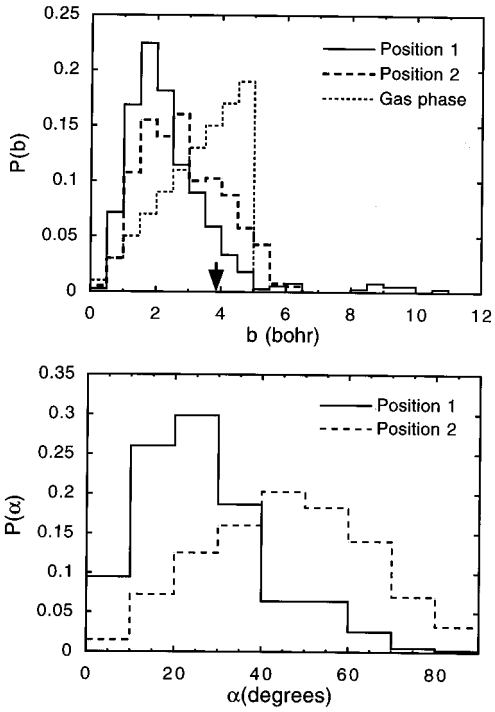

Figure 4. Impact parameter (upper panel) and incident angle (lower panel) distributions produced by trajectories in position 1 (solid line) and position 2 (dashed line). The short dashed line in the upper panel and the arrow indicate the distribution of the impact parameter and the maximum impact parameter for reactive trajectories in the gas-phase simulation.[12] All distributions are presented as fractions of the total number of trajectories.

because of the closeness of the H and CO_2 on the surface. Due to the initial HBr adsorption configuration, the dissociated H atom is usually scattered by the surface before colliding with a coadsorbed CO_2. Typically, the hydrogen after the surface scattering finds itself in the region approaching the barrier to reaction, with a potential energy of perhaps several tenths of an electronvolt. Since it has not yet surmounted the barrier to the HOCO complex, the concept of an impact parameter and incident angle still has some validity.

It is difficult to extract information on the distribution of these two parameters because the scattering of the hydrogen by the surface and its interaction with CO_2 are not always separable. In a similar study, Barclay et al.[19] attempted to determine the impact parameter immediately after the *z*-component of the H velocity changes its sign. However, our analyses show that this approach does not always yield unique results, largely because the surface scattering in their calculations as in ours is not an instantaneous process and the direction of the H velocity changes gradually during the scattering. In our calculations, we took a new strategy: a different batch of trajectories was calculated with the H−CO_2 interaction switched off. The *b* and α were then calculated when the H is 3.4 bohr above the surface, the height at which the H was situated before the photodissociation. The calculated distributions are given in Figure 4 for positions 1 and 2.

From the gas-phase simulations, it is known that the distribution of reactive trajectories is essentially flat until *b* reaches 3.8 bohr and then falls off quickly to zero.[12] Hence, a maximum impact parameter of 5 bohr was used in the gas-phase simulation to cover the space that may lead to reaction. In gas-phase conditions, the distribution of impact parameters for all collisions, both reactive and nonreactive, increases linearly with *b*. This means that collisions with impact parameters small enough to allow reaction to occur are highly improbable. By contrast, the impact parameters for well-aligned reactants on the surface

TABLE 4: Energy Partitioning for Desorbed Products at 193 nm

	position		
	1	2	gas phase[12]
$\langle E_T^{CO}\rangle$[a]	0.30	0.25	
$\langle E_{vib}^{CO}\rangle$	0.33	0.28	0.40
$\langle E_{rot}^{CO}\rangle$	0.17	0.16	0.18
$\langle \nu^{CO}\rangle$	0.83	0.64	1.06
$\langle J^{CO}\rangle$	22.0	22.0	24
$\langle E_T^{OH}\rangle$	0.42	0.47	
$\langle E_{vib}^{OH}\rangle$	0.41	0.38	0.26
$\langle E_{rot}^{OH}\rangle$	0.33	0.34	0.33
$\langle \nu^{OH}\rangle$	0.45	0.48	0.17
$\langle N^{OH}\rangle$	10.3	10.5	10

[a] Energy unit in eV.

are small enough to make reaction possible. This is shown in the upper panel in Figure 4. The distributions for both positions peak around $b = 2-3$ bohr and decrease quickly. The distribution for position 2 favors somewhat larger impact parameters, which is consistent with the lower reactivity in this position. The small impact parameter for the surface-aligned reaction is a contributing factor for the enhanced reactivity.

Another factor affecting the likelihood of reaction in the gas-phase simulation is the incident angle α, which reflects the anisotropy of the interaction potential. The gas-phase simulation with random sampling of all the angles showed that the reactivity peaks in the ranges $20° < \alpha < 30°$ and $70° < \alpha < 80°$,[12] indicating some stereoselectivity. The first range corresponds to the near-collinear H···OCO attack, leading to the *cis*−*trans* HOCO complex, while the second range corresponds to the formation of the T-shaped HCO_2 complex. While the α sampling for the gas-phase reaction is uniformly distributed, the distribution for the surface-aligned reaction is certainly nonuniform. The lower panel of Figure 4 displays the α distribution for all the trajectories. For position 1, the distribution peaks near the HOCO entrance channel at 20−30°, and few trajectories are generated with α corresponding to the T-shaped HCO_2 complex. As a result, the H attack is concentrated on a specific alignment which is known to be more reactive. However, the distribution for position 2 peaks at 40−60°, where the gas-phase simulation shows little reactivity. The distribution is broad and gives slightly better overlap with the T-shaped entrance channel than does position 1. However, overlap with the linear HOCO channel is diminished. Thus, position 1 is more favorably aligned for reaction than is position 2. Our analyses also indicate that the low reactivity in positions 3 and 4 can be attributed to the large impact parameter or to misalignment of the adsorbates. Overall, the results strongly suggest that the enhancement of reactivity is intimately related to the impact parameter and alignment.

(b) Product-State Distributions. After the propagation is terminated, the translational, rotational, and vibrational energies of the desorbed diatomic products are calculated. The sign of the center-of-mass velocity of a product along the surface normal is used to determine if the molecule desorbs. It was found that 95% (90%) of OH and 63% (57%) of CO desorb for position 1 (position 2). The rotational and vibrational quantum numbers of the diatoms are extracted by using a binning scheme. The internal state distribution of the unreactive CO_2 is not analyzed here. Table 4 displays the calculated mean translational, vibrational, and rotational energy and the corresponding quantum numbers for the two diatomic products in the reactive channel. For comparison purposes, the gas-phase results of Kudla and Schatz[12] at 2.54 eV are also included in the table. The results are all generated from approximately 1000 trajectories. As shown in Table 4, the averaged energy partitioning and averaged quantum numbers are very similar for the two

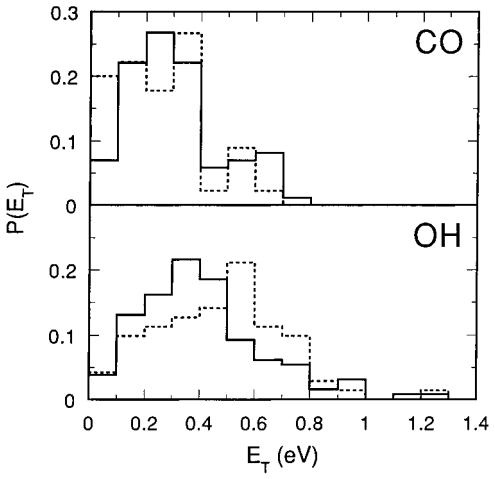

Figure 5. Translational energy distributions of the desorbed diatomic products as fractions of the total reactive trajectories. The solid line represents position 1, and the dotted line position 2.

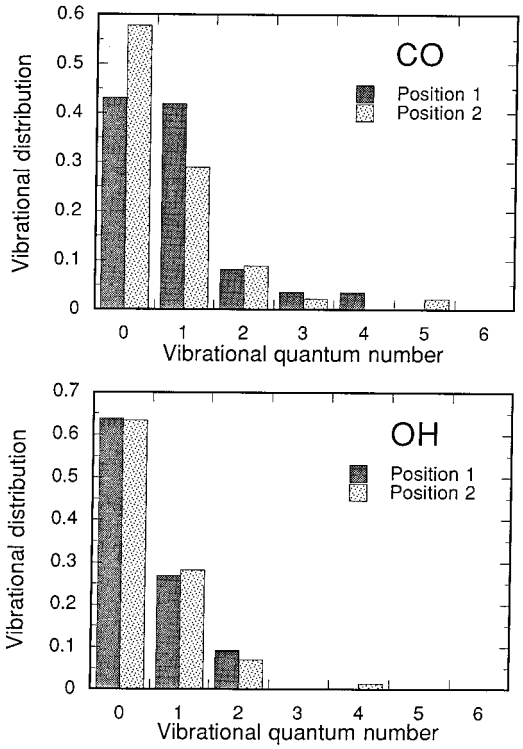

Figure 6. Vibrational state distributions of the desorbed diatomic products.

adsorption positions. They are also very close to the gas-phase results. For the CO molecule, it appears that its vibrational excitation from the surface reaction is slightly less pronounced than its gas-phase counterpart. The insensitivity of the final state distributions to initial configuration is an indication that the long-lived complex formation erases the memory of the entrance channel.

The translational energy distributions of the desorbed CO and OH products, displayed in Figure 5, are similar for both positions. The majority of the CO product falls under 0.4 eV and a tail extends to near 0.8 eV. The OH distributions peak slightly higher for position 1 than for position 2. The vibrational state distributions of the desorbed CO and OH products are shown in Figure 6 for both adsorption positions, and they are remarkably similar. The ground vibrational state of both products represents the largest fraction while vibrational excitation also exists. The rotational distribution of CO is rather diffused and extends to $J = 60$, as shown in Figure 7, while

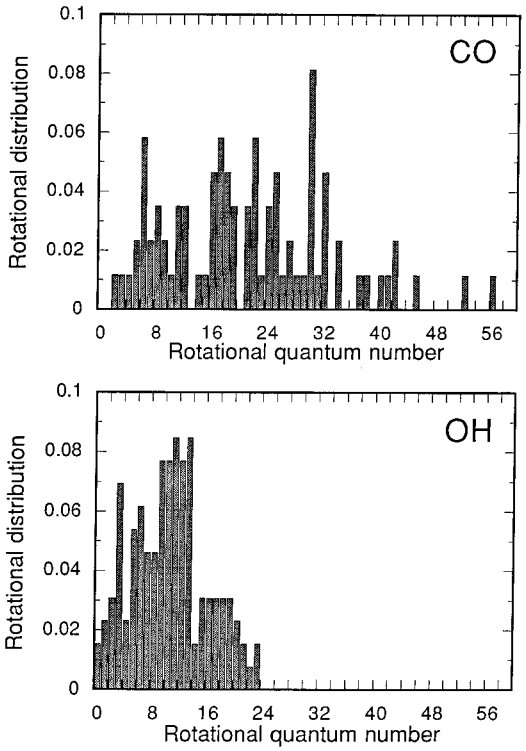

Figure 7. Rotational state distributions of the desorbed diatomic products. The results for positions 1 and 2 are similar, and only the distributions for the former are shown.

the OH distribution peaks at approximately $N = 10$ and has a clear cutoff at 25. The distributions for both positions are quite similar and only the distributions for position 1 are given here.

To further analyze the reactive trajectories, we plot in Figure 8 the product distribution in both the polar (θ) and azimuthal (ϕ) angles for all the reactive trajectories. More than two-thirds of the CO product trajectories recoil at θ angles greater than or equal to 60° for both positions, giving a large velocity component parallel to the surface plane. By contrast, a substantial proportion of the OH product desorbs at angles closer to the surface normal, with the angle peaking around 40−50°. As a result, the majority (~90%) of OH products desorb while a much smaller portion of CO products (~60%) escape. Both positions yield a peak in the ϕ distribution for CO which is consistent with the orientation of CO_2 before reaction. In position 1 the CO_2 molecule is aligned with the *y* axis and the CO fragment also departs along the *y* axis at 270°. In position 2 the molecule is aligned at 45° with the *x* axis, while CO escapes around 20−40° from the *x* axis ($\phi = 320-340°$). The ϕ distribution for OH is flat over most of the range. The ϕ distribution of CO is the only final attribute possessing some memory of the initial configuration.

(c) Lifetimes. The average lifetime of the reactive trajectories, which is defined as the time span between the photodissociation of HBr and the separation of the products to a distance of 12 bohr, is 0.4 ps, slightly higher than that found in the gas-phase simulation (0.3 ps) at a similar energy (2.54 eV).[12] It is conceivable that the prolonged lifetime of the surface reaction is due to the blocking of the exit channel by the surface. Figure 9 indicates that most nonreactive trajectories have relatively short lifetimes (<100 fs). Fewer than 10% of the nonreactive trajectories pass through complexes, a small number of which lasts longer than 0.5 ps. The reactive trajectories, on the other hand, typically have significantly longer lifetimes due to complex formation. For these trajectories, the lifetime is sufficiently long to erase memory of the entrance channel and

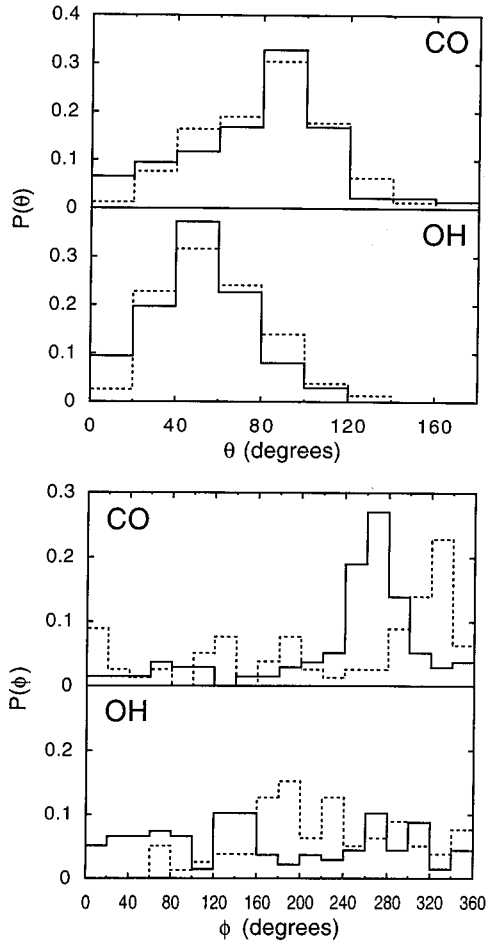

Figure 8. Angular distributions in θ and ϕ for all the diatomic products. The angles are defined in Figure 3. The solid line represents position 1, and the dotted line position 2.

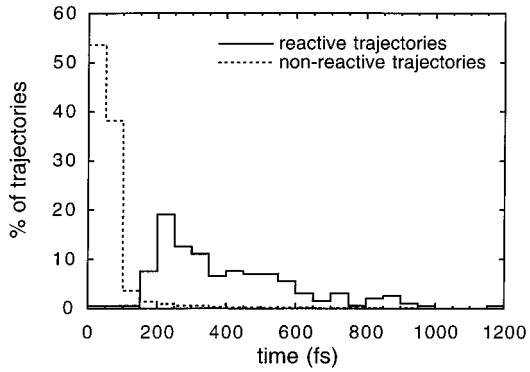

Figure 9. Lifetime distribution of all the trajectories. The solid line denotes the percentage of reactive trajectories with a given lifetime, while the dotted line gives the percentage of nonreactive trajectories.

to move toward a near statistical distribution of the energy among all degrees of freedom.

(d) Nonreactive Scattering. Nonreactive trajectories fall into two groups: those that have formed complexes and those that have not. Hydrogen may surmount the energy barrier and form a complex, only to depart later without leading to products. If the complex lasts for several vibrational periods, the H atom will depart at an angle that bears little relation to the incident angle and its energy may have been thermalized by the complex. However, when the incoming hydrogen atom does not have enough energy to pass over the barrier, we have in effect a simple scattering event as the hydrogen atom bounces off the CO_2 molecule at an angle and energy that give evidence of its origin. As shown in Figure 9, most of the trajectories are

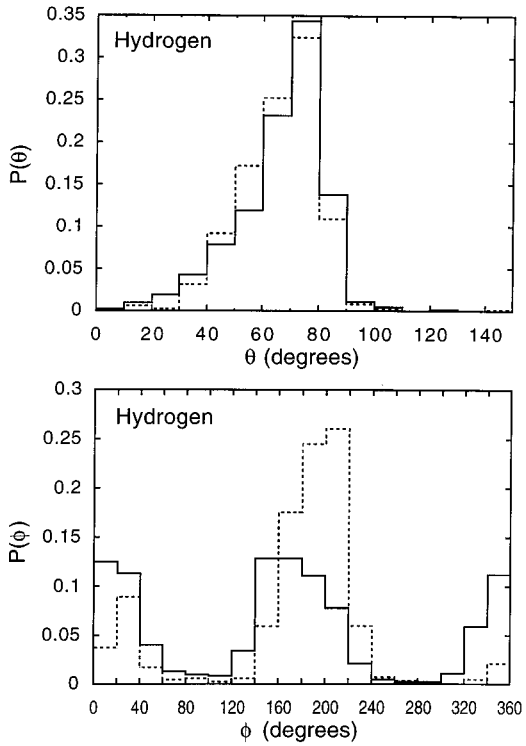

Figure 10. Angular distributions in θ and ϕ for the hydrogen scattered in nonreactive trajectories. The solid line represents position 1 and the dotted line position 2.

completed in less than 100 fs, and the hydrogen atom is directly scattered by CO_2.

The angular distributions for the nonreactive hydrogen atom are shown in Figure 10. Both adsorption positions show hydrogen atoms escaping in two opposite ϕ directions, 0° and 180°. Very few atoms move along the *y*-axis (near 90° and 270°) because these directions are effectively blocked by the presence of the CO_2 molecule and the bromine atom, both of which are bulky compared to the hydrogen atom. These entities form, in effect, an incomplete cage from which the hydrogen atom can escape only through its open sides along the *x*-axis. The θ distribution peaks around 70−80° for both positions, indicating that these atoms are departing the cage at an angle close to the surface plane. This makes it likely that the atom can experience subsequent collisions with another coadsorbate lying to either side of the cage. If the atom retains sufficient energy, reaction may be possible during this secondary encounter. The translational energy distribution for the nonreactive hydrogen atom (upper panel of Figure 11) shows a significant portion with high energy. Both positions produce similar distributions peaked near 2.5 eV with most trajectories falling between 0.5 and 3.0 eV. About three-fourths have energy above 1.5 eV, higher than the minimum energy barrier for the H + CO_2 reaction. The cutoff of the H translational energy distribution is slightly higher than that obtained from the isolated HBr photodissociation (2.61 eV). This increase is probably due to the energy transfer from CO_2 to the scattered H.

An examination of the scattering behavior of the hydrogen atom leads to some useful information concerning the role of the surface in the dynamics of the reaction and has implications for using the surface as a template for reactivity enhancement. As we have already seen in Figure 11, the scattered hydrogen atoms cover a wide range of energy values, and some atoms lose a large amount of energy. Since the surface is rigid in this model, energy loss to the surface is not a factor. The atom can lose energy upon collision with the CO_2 molecule, and differences in the geometry of the attack and the vibrational

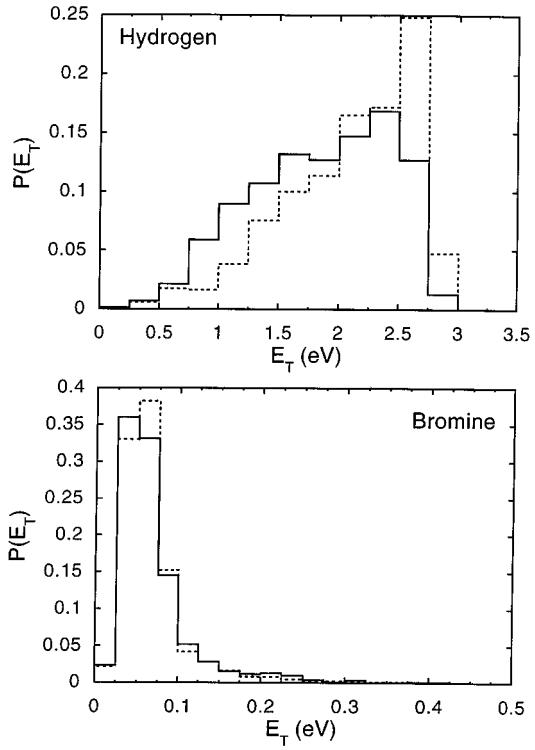

Figure 11. Translational energy distributions of the hydrogen atom (upper panel) and the bromine atom (lower panel) produced in nonreactive trajectories. The solid line represents position 1 and the dotted line position 2.

phase of the molecule can cause a wide variation in the amount of energy transferred. In addition, those H atoms that form a HOCO complex and later escape may also have smaller translation energies. A second mechanism for energy loss is suggested by the correlation between the translational energy of the H atom and the angle of departure, θ. Our results show that hydrogen atoms emerging from the surface close to the surface normal ($\theta < 20°$) all have experienced significant energy loss and their distribution in the angle ϕ is more nearly isotropic than those atoms emerging at large angles to the surface normal. Both facts suggest that this component of the scattered hydrogen has experienced a secondary collision after bouncing off of CO_2. Since energy loss to the surface is not permitted by this model, collision with the bromine atom is the likely candidate for such a collision. Analyses of trajectories confirm the chattering of hydrogen inside the cage. The energy distribution for the bromine atom (lower panel in Figure 11) displays a high-energy tail, which is consistent with such a mechanism. Similar events in surface photodissociation have been discussed extensively before.[47−49,55−58] Hydrogen atoms undergoing such chattering would likely become unavailable for reaction during subsequent encounters with coadsorbed CO_2, both due to the energy loss and the angle of departure.

Chattering is, however, a relatively rare event, occurring in only a few percent of the trajectories. However, Figure 11 shows a very large proportion of the bromine atoms with energy higher than the limit produced by photodissociation in the gas phase (0.032 eV). About 75% of the trajectories occur between 0.03 and 0.1 eV. Another mechanism for energy transfer to bromine is operating in a large majority of trajectories. The "squeezed atom effect" is a likely candidate. Since the reactants are brought close together by adsorption on the surface, the dissociating hydrogen atom begins feeling the repulsion from CO_2 even before it is completely free of repulsion from bromine. The bromine atom, in effect, pushes against not only the hydrogen atom but also the CO_2 molecule. The hydrogen atom squeezed between the two more massive entities can transfer energy between them. Classical trajectory studies on photodissociation of the HBr·CO_2 van der Waals complex show that the products receive only 80−90% of the energy that they would receive in the gas-phase reaction.[12] This implies that bromine receives the other 10−20% of the energy. If the hydrogen atom carries less energy to the CO_2 molecule than it does in the gas-phase reaction, we might expect a reduction in reactivity, since the reaction is endoergic with a large energy barrier to complex formation. We tested this effect by performing the same simulation with the Br−CO_2 interactions turned off. The reactivity increases by about one-fifth. The squeezed atom effect may also operate as the hydrogen moves between bromine and the surface immediately after photodissociation begins.

Another factor impacting the use of the surface to align reactants is the directional character of the scattering of the reagent atom by the surface. In this case, the reagent atom is small enough to experience the corrugation of the surface, and reflection is not expected to be specular. Due to thermal motion of the HBr molecule, the hydrogen atom can contact a range of points on the curved surface of the surface ion. The result is a broadened range of reflection in both the θ and ϕ angles (not shown here). In this study, the ϕ distribution of the hydrogen atom before impact with the surface has a standard deviation of 8.2°, due to thermal motion of the parent molecule on the surface. After reflection at the surface the ϕ distribution broadens, yielding a 13.3° standard deviation. The initial standard deviation in θ is 5.8° and increases to 7.4°. If we hope to target a precisely chosen location, this effect may reduce the reactivity. However, in the likely event that a given surface does not bring the reactants into perfect alignment, such a broadened range of attack has a better chance of overlapping a favorable entrance channel.

V. Concluding Remarks

Our calculations have illustrated the potentially useful scheme, first proposed by Polanyi,[13] to enhance and/or control the reactivity of a chemical reaction by using insulator surfaces as templates. In particular, we have demonstrated that it is possible to enhance the reactivity between photolytically prepared H and adsorbed CO_2. Because the physisorbed reactants are held in close proximity on the surface by weak forces, the impact parameter for the reaction is necessarily small, which favors the reactive channel. Our results also indicate that the alignment of the adsorbates prior to reaction plays an important role in determining the reactivity. The energy of the incident reactant, H in this study, can be controlled because the reaction is initiated by a photon. Since the surface provides only a template for the reaction, one has the freedom to select different insulator surfaces and different crystal faces. The lattice constant of a particular surface can thus be utilized to adjust the relative distance and alignment of the two coadsorbates. The scheme employed here should be robust and extendible to other systems. For example, HX can be replaced by another hydrogen containing molecule, such as H_2S, which also dissociates to yield a fast hydrogen atom upon photoabsorption. Because of the different adsorption geometry, one can effectively change the alignment of the co-adsorbates and thus the outcome of the reaction. In many respects, the reaction studied here is not an ideal model to demonstrate the advantages of the surface-aligned reaction because of its endothermicity and complex formation. One can presumably achieve more in systems that have large anisotropy and exothermicity. In summary, the scheme may open a new gateway for manipulating chemical reactions. It may also find wide applications in many surface chemical processes, such as photoetching, chemical vapor deposition, etc.

A shortcoming of the present study is the possible inaccuracy of the empirical potentials used in the calculation, although they have been tested in prior theoretical investigations where comparison with experimental data are available. Better knowledge of the interaction potential can be achieved by experimental measurements and by *ab initio* calculations. Apart from the apparent need to improve the quality of the interaction potential, we identify the following important aspects. First, the motion of the surface ions should be included, which will certainly give a more realistic representation of the dynamics. Second, the number of adsorbates on the surface should be increased to include secondary collisions for the energetic H atoms and to allow for more realistic modeling of adsorbate−adsorbate interactions. In addition, dynamics at different photon frequencies will allow exploration of different regions of the potential energy surface and yield a more complete picture of the dynamics. It can be expected that the dynamics will be more complex than the results reported here when these factors are taken into account. Nevertheless, the major conclusions reached in this work are expected to prevail. Work in these directions will be published elsewhere.[59]

Finally, we want to emphasis that this work is an exploratory study designed to assess the possibility of the surface-aligned photochemical reaction of the $H + CO_2$ system on LiF(001). It is our hope that this work will be able stimulate some experimental interest in this system. It is, of course, highly likely that the quantitative predictions obtained in our calculations may require significant modifications by future experimental and theoretical investigations. However, the interplay between experiment and theory will certainly enhance our understanding of surface photochemical dynamics.

Acknowledgment. We acknowledge financial support from the National Science Foundation (CHE-9411934 to H.G. and CHE-9527677 to G.C.S.). Partial support from the Petroleum Research Fund administered by the American Chemical Society is also acknowledged. The calculations were performed on the Cray YMP at the Ohio Supercomputer Center.

References and Notes

(1) Somorjai, G. A. *Introduction to Surface Chemistry and Catalysis*; Wiley: New York, 1994.
(2) Levine, R. D.; Bernstein, R. B. *Molecular Reaction Dynamics and Chemical Reactivity*; Oxford University Press: Oxford, 1991.
(3) Orr-Ewing, A. J. *J. Chem. Soc., Faraday Trans.* **1996**, *92*, 881.
(4) Sinha, A.; Hsiao, M. C.; Crim, F. F. *J. Chem. Phys.* **1991**, *94*, 4928.
(5) Bronikowski, M. J.; Simpson, W. R.; Zare, R. N. *J. Phys. Chem.* **1993**, *97*, 2194 1993.
(6) Greene, C. H.; Zare, R. N. *Annu. Rev. Phys. Chem.* **1982**, *33*, 119.
(7) Gandhi, S. R.; Curtiss, T. J.; Bernstein, R. B. *Phys. Rev. Lett.* **1987**, *59*, 2951.
(8) Wittig, C.; Sharpe, S.; Beaudet, R. A. *Acc. Chem. Res.* **1988**, *21*, 341.
(9) Chen, Y.; Hoffman, G.; Shin, S. K.; Oh, D.; Sharpe, S.; Zeng, Y. P.; Beaudet, R. A.; Wittig, C. In *Advances in Molecular Vibrations and Collision Dynamics*; JAI Press Inc.: Greenwich, CT, 1991; Vol. 1B, pp 187−229.
(10) Shin, S. K.; Chen, Y.; Nickolaisen, S.; Sharpe, S. W.; Beaudet, R. A.; Wittig, C. In *Advances in Photochemistry*; Volman, D., Hammond, G., Neckers, D., Eds.; Wiley: New York, 1991; p 249.
(11) Schatz, G. C.; Fitzcharles, M. S. In *Selectivity in Chemical Reactions*; Whitehead, J. C., Ed.; Kluwer Academic Publishers: Dordrecht, 1988; p 353.
(12) Kudla, K.; Schatz, G. C. *J. Phys. Chem.* **1991**, *95*, 8267.
(13) Polanyi, J. C.; Williams, R. J. *J. Chem. Phys.* **1988**, *88*, 3363.
(14) Polanyi, J. C.; Rieley, H. in *Dynamics of Gas-Surface Interactions*; Rettner, C. T., Ashfold, M. N. R., Eds.; The Royal Society of Chemistry: Cambridge, 1991.
(15) Guo, H.; Setzler, J. V. *Hetero. Chem. Rev.* **1995**, *2*, 17.
(16) Bourdon, E. B. D.; Das, P.; Harrison, I.; Polanyi, J. C.; Segner, J.; Stanners, C. D.; Williams, R. J.; Young, P. A. *Faraday Discuss. Chem. Soc.* **1986**, *82*, 343.
(17) Harrison, I.; Polanyi, J. C.; Young, P. A. *J. Chem. Phys.* **1988**, *89*, 1498.
(18) Barclay, V. J.; Hung, W.-H.; Keogh, W. J.; Kühnemuth, R.; Polanyi, J. C.; Zhang, G.; Zeiri, Y.; Jennison, D. R.; Li, Y. S. *J. Chem. Phys.* **1996**, *105*, 5005.
(19) Barclay, V. J.; Jack, D. B.; Polanyi, J. C.; Zeiri, Y. *J. Phys. Chem.* **1993**, *97*, 12541.
(20) Flynn, G. W. *Science* **1989**, *246*, 1009.
(21) Scherer, N. F.; Sipes, C.; Bernstein, R. B.; Zewail, A. H. *J. Chem. Phys.* **1990**, *92*, 5239.
(22) Rice, J. K.; Baronavski, A. P. *J. Chem. Phys.* **1991**, *94*, 1006.
(23) Alagia, M.; Balucani, N.; Casavecchia, P.; Stranges, D.; Volpi, G. G. *J. Chem. Phys.* **1993**, *98*, 8341.
(24) Ionov, S. I.; Brucker, G. A.; Jaques, C.; Valachovic, L.; Wittig, C. *J. Chem. Phys.* **1993**, *99*, 6553.
(25) Schatz, G. C.; Fitzcharles, M. S.; Harding, L. B. *Faraday Discuss. Chem. Soc.* **1987**, *84*, 359.
(26) Kudla, K.; Schatz, G. C.; Wagner, A. F. *J. Chem. Phys.* **1991**, *95*, 1635.
(27) Kudla, K.; Schatz, G. C. In *The Chemical Dynamics and Kinetics of Small Radicals*; Liu, K., Wagner, A. F., Eds.; World Scientific: 1995; p 438.
(28) Schatz, G. C.; Dyck, J. *Chem. Phys. Lett.* **1992**, *188*, 11.
(29) Clary, D. C.; Schatz, G. C. *J. Chem. Phys.* **1993**, *99*, 4578.
(30) Goldfield, E. M.; Gray, S. K.; Schatz, G. C. *J. Chem. Phys.* **1995**, *102*, 8807.
(31) Blass, P. M.; Jackson, R. C.; Polanyi, J. C.; Weiss, H. *J. Chem. Phys.* **1991**, *94*, 7003.
(32) Polanyi, J. C.; Williams, R. J.; O'Shea, S. F. *J. Chem. Phys.* **1991**, *94*, 978.
(33) Huang, Z.-H.; Guo, H. *J. Chem. Phys.* **1992**, *96*, 8564.
(34) Bourdon, E. B. D.; Cho, C.-C.; Das, P.; Polanyi, J. C.; Stanners, C. D.; Xu, G.-Q. *J. Chem. Phys.* **1991**, *95*, 1361.
(35) Berg, O.; Ewing, G. E. *Surf. Sci.* **1989**, *220*, 207.
(36) Heidberg, J.; Kampshoff, E.; Schönekäs, O.; Stein, H.; Weiss, H. *Ber. Bunsen-Ges. Phys. Chem.* **1990**, *94*, 118.
(37) Heidberg, J.; Kampshoff, E.; Schönekäs, O.; Stein, H.; Weiss, H. *Ber. Bunsen-Ges. Phys. Chem.* **1990**, *94*, 112.
(38) Heidberg, J.; Kampshoff, E.; Kühnemuth, R.; Schönekäs, O. *Surf. Sci.* **1991**, *251/252*, 314 1991.
(39) Heidberg, J.; Kampshoff, E.; Kühnemuth, R.; Schönekäs, O. *Surf. Sci.* **1992**, *272*, 306.
(40) Lange, G.; Schmicker, D.; Toennies, J. P.; Vollmer, R.; Weiss, H. *J. Chem. Phys.* **1995**, *103*, 2308.
(41) Heidberg, J.; Kampshoff, E.; Schönekäs, O.; Stein, H.; Weiss, H. *Ber. Bunsen-Ges. Phys. Chem.* **1990**, *94*, 127.
(42) Hu, W.; Saberi, M.-A.; Jakalian, A.; Jack, D. B. *J. Chem. Phys.* **1997**, *106*, 2547.
(43) Heidberg, J.; Singh, R. K.; Chen, C. F. *Z. Phys. Chem. N. F.* **1978**, *110*, 135.
(44) Steele, W. A.; *The Interaction of Gases with Solid Surfaces*; Pergamon: New York, 1974.
(45) Spackman, M. A. *J. Chem. Phys.* **1986**, *85*, 6579.
(46) Chapman, D. A.; Balasubramanian, K.; Lin, S. H. *Phys. Rev. A* **1988**, *38*, 6098.
(47) Huang, Z.-H.; Guo, H. *J. Chem. Phys.* **1992**, *97*, 2110.
(48) Huang, Z.-H.; Guo, H. *J. Chem. Phys.* **1993**, *98*, 3395.
(49) Setzler, J. V.; Huang, Z.-H.; Guo, H. *J. Chem. Phys.* **1995**, *103*, 4300.
(50) Allen, M. P.; Tildesley, D. J. *Computer Simulation of Liquids*; Oxford University Press: Oxford, 1986.
(51) Wilson, E. B.; Decius, J. C.; Cross, P. C. *Molecular Vibrations*; Dover: New York, 1955.
(52) Tully, J. C.; Preston, R. K. *J. Chem. Phys.* **1971**, *55*, 562.
(53) Nikitin, E. E.; Zulicke, L. *Theory of Chemical Elementary Processes*; Springer-Verlag: Berlin, 1978.
(54) Truhlar, D. G.; Muckerman, J. T. In *Atom-Molecule Collision Theory*, Bernstein, R. B., Ed.; Plenum: New York, 1979.
(55) Guo, H.; Schatz, G. C. *J. Chem. Phys.* **1991**, *94*, 379.
(56) Guo, H.; Schatz, G. C. *Chem. Phys. Lett.* **1991**, *184*, 245.
(57) Harrison, I.; Polanyi, J. C.; Young, P. A. *J. Chem. Phys.* **1988**, *89*, 1475.
(58) Fairbrother, D. H.; Briggman, K. A.; Stair, P. C.; Weitz, E. *J. Chem. Phys.* **1995**, *102*, 7267.
(59) Setzler, J. V.; Bechtel, J.; Guo, H.; Schatz, G. C. *J. Chem. Phys.*, to be submitted.